

## RESEARCH ARTICLE

# High efficiency screen printed bifacial solar cells on monocrystalline CZ silicon

L. Yang<sup>1\*</sup>, Q.H. Ye<sup>1</sup>, A. Ebong<sup>2</sup>, W.T. Song<sup>3</sup>, G.J. Zhang<sup>3</sup>, J.X. Wang<sup>3</sup> and Y. Ma<sup>3</sup><sup>1</sup> Solar Energy Institute of the Physics Department, Shanghai Jiao Tong University, Shanghai, PR China<sup>2</sup> University Center of Excellence for Photovoltaic Research and Education, School of Electrical and Computer Engineering, Georgia Institute of Technology, 777 Atlantic Drive, Atlanta, GA 30332-0250, USA<sup>3</sup> Solarfun Co., Ltd, Linyang Road 666, Qidong, Jiangsu, China

## ABSTRACT

We present industrialized bifacial solar cells on large area (149 cm<sup>2</sup>) 2 cm CZ monocrystalline silicon wafers processed with industrially relevant techniques such as liquid source BBr<sub>3</sub> and POCl<sub>3</sub> open-tube furnace diffusions, plasma enhanced chemical vapor deposition (PECVD) SiN<sub>x</sub> deposition, and screen printed contacts. The fundamental analysis of the paste using at boron-diffused surface and the bifacial solar cell firing cycle has been investigated. The resulting solar cells have front and rear efficiencies of 16.6 and 12.8%, respectively. The ratio of the rear J<sub>SC</sub> to front J<sub>SC</sub> is 76.8%. It increases the bifacial power by 15.4% over a conventional solar cell at 20% of 1-sun rear illumination, which equals to the power of a conventional solar cell with 19.2% efficiency. We also present a bifacial glass–glass photovoltaic (PV) module with 30 bifacial cells with the electrical characteristics. Copyright © 2010 John Wiley & Sons, Ltd.

## KEYWORDS

bifacial; boron diffusion; screen-printing

### \*Correspondence

L. Yang, Solar Energy Institute of the Physics Department, Shanghai Jiao Tong University, Shanghai, PR China.

E-mail: le\_yang@hotmail.com

Received 22 December 2009; Revised 24 May 2010

## 1. INTRODUCTION

The search for a continued reduction of the cost of photovoltaic (PV) electricity has led to considerable effort on the reduction of silicon (Si) consumption via the use of thin Si wafers. Wafers below 180 μm in thickness introduce a number of challenges. Device efficiencies (Eff) become increasingly dependent on surface conditioning and passivation requiring surface engineering. In addition, during thin wafer large volume manufacturing wafers become susceptible to warping and breakage during both cell and module manufacturing.[1,2] To realize the theoretical efficiency limit of a silicon solar cell, the backside aluminum must be replaced with dielectric and local contacts.[3] To accomplish this, boron becomes an alternative material to provide the back surface field (BSF) for p-type substrate and p-n junction on n-type silicon solar cells.[4,5] Also, the bowing of the conventional full aluminum rear surface is the critical problem that needs to be solved.[6] The use of boron BSF can avoid the bowing and set the stage for higher efficiency.

Bifacial solar cell is of great interest because of the higher efficiency potential and the need to improve solar cell power generation.[7] The bifacial structure having metal gridlines on both surfaces can receive sunlight from both sides and create under certain conditions 20% more power than the single sided counterpart. An additional advantage of the bifacial solar cell over the conventional is the reduction in cell temperature due to the reduced heat absorption in the absence of the Al back metallization. This is important in field operation of the module with bifacial cells, which can run at lower temperature than the conventional modules, and upholds higher maximum power.

This work presents an industrialized low-cost screen-printed process that yields bifacial solar cells on CZ monocrystalline substrates (Figure 1). Progress on research has also been achieved in this area recently.[8,9] The primary challenges associated with screen-printed CZ bifacial solar cells are the BBr<sub>3</sub> boron diffusion, boron-diffused surface passivation, and metallization. It is known that junction depth, surface carrier concentration, sheet resistance, and diffusion uniformity control the dark

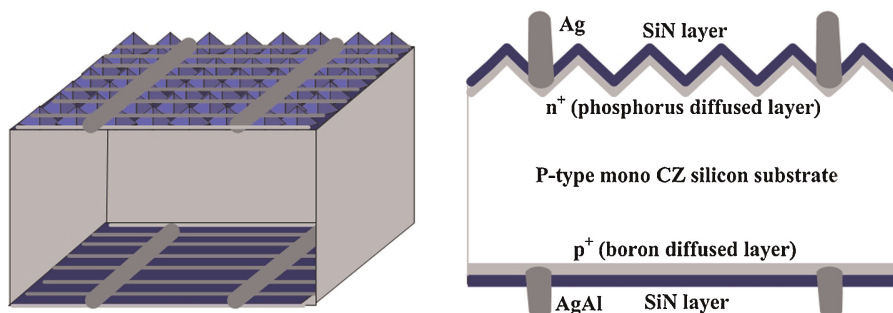


**Figure 1.** Schematic diagram of the bifacial solar cell with  $p^+pn^+$  structure.

saturation current density  $J_0$  and the effective lifetime in silicon solar cells.[10] As part of this work boron diffusion conditions have been tailored in order to achieve critical cell physical parameters necessary for bifacial operation. Furthermore, we have shown that plasma enhanced chemical vapor deposition (PECVD) silicon nitride layer can mask against cross-diffusion during the boron and phosphorus diffusion processes.

## 2. EXPERIMENTAL

We need to diffuse two different impurities phosphorus and boron into front and rear surface separately to achieve the bifacial solar cell  $p^+pn^+$  or  $p^+nn^+$  structure. Boron and phosphorus diffusions were performed in a tube furnace employing liquid sources:  $BBr_3$  liquid source for boron and  $POCl_3$  liquid source for phosphorus. To achieve comparable junction characteristics, boron diffusion in Si requires much higher diffusion temperatures than phosphorus diffusion in Si.[11,12] As a means to assure optimum boron and phosphorus diffusion conditions minimizing their impact on the post-diffusion wafer lifetime, we measured the effective minority carrier lifetime as a function of the excess minority carrier density  $\Delta n$  (at  $10^{15} \text{ cm}^{-3}$  injection level) using the quasi-steady-state photoconductance (QSS-PC) technique.[13]

In this work, we used  $200 \mu\text{m}$  thick  $2 \Omega \text{ cm}$  p-type Czochralski silicon wafers. After saw damage removal, substrates were cleaned by standard ratio corporation of America (RCA) clean. Next, boron diffusion was performed in a conventional tube furnace using  $BBr_3$  liquid source at a set temperature of  $1020^\circ\text{C}$ . This was followed by the boron glass removal and deionized (DI) water rinse before the PECVD  $\text{SiN}_x$  anti-reflection coating and masking layer was deposited; layer thickness was optimized to guarantee the adequate masking of the subsequent phosphorus diffusion. Afterwards, the front side alkaline texturing was performed prior to phosphorus diffusion using  $POCl_3$ . The rest of the process steps are outlined in Table I. The diffusion profiles were measured using spreading resistance analysis (SRA) with  $1 \mu\text{m}$   $x$ -step increments to understand the surface concentration and junction depths (Figure 2).

Understanding the back and front conductor paste properties and their interaction with the co-firing step is critical to getting high quality screen-printed contacts. The contact resistance at the front and rear must be low. Thus, the use of an appropriate rear contact conductor paste and optimized firing cycle is critical to proper solar cell operation.[14] To achieve this we used a co-firing condition for conventional Al-BSF cells. Since aluminum surface for a standard Al-BSF cell and the  $\text{SiN}_x$  dielectric for the

**Table I.** Processing sequence for bifacial solar cells.

Process sequence	Process description
I	Substrate chemical polish/RCA standard clean
II	$BBr_3$ boron diffusion (face to face)
III	$\text{SiN}$ deposition on boron-diffused side ( $p^+$ side)
IV	Alkaline texturing
V	$POCl_3$ diffusion (back to back)
VI	$\text{SiN}$ deposition on phosphorus-diffused side ( $n^+$ side)
VII	Screen-printing of AgAl paste on $p^+$ surface and drying
VIII	Screen-printing of Ag paste on $n^+$ surface
IX	Co-firing of the contacts

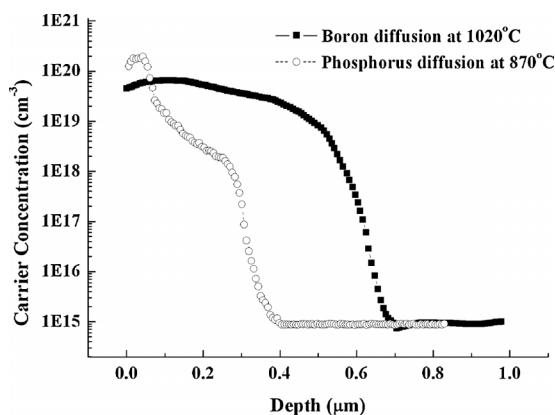


**Figure 2.** Boron and phosphorus carrier concentrations determined by SRA.

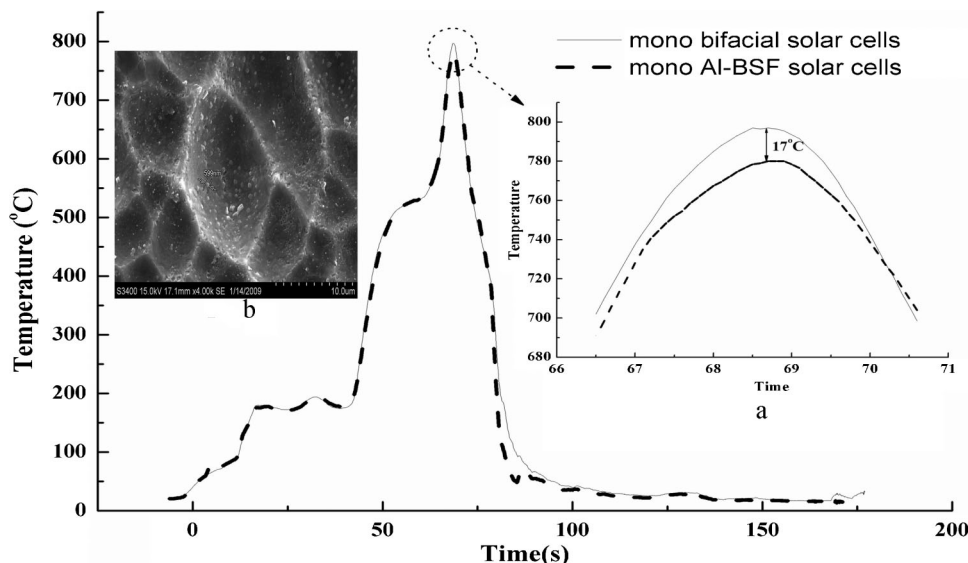


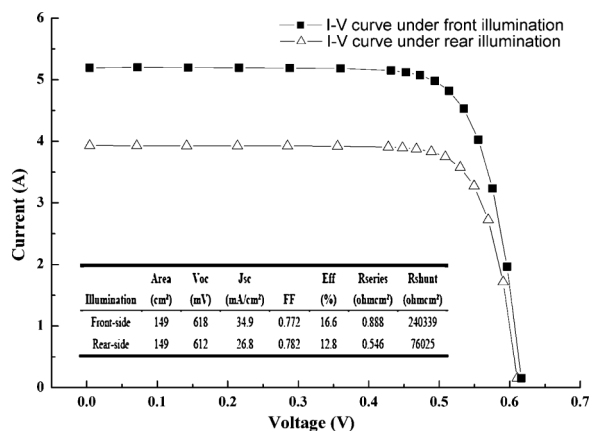
**Figure 3.** Comparison diagrams of the measured bifacial solar cell firing curve and the conventional Al-BSF solar cell at same firing process condition. (a) Zooms into the firing peak temperature profile indicating the differences in temperature during the firing of the bifacial and conventional cells fabricated in this study. (b) SEM image of the silver–aluminum paste at the boron-diffused silicon surface after metal etching showing a large density of Ag–Si crystallites.

bifacial cell design have different heat absorption coefficients, the monofacial and bifacial solar cells will experience different peak temperatures for the same set points as shown in Figure 3. Silver–silicon island size and distribution are heavily impacted by paste formulation and the firing process and play a critical role in defining contact resistance.[15,16] Figure 3b shows SEM surface image of the boron-diffused surface after contact formation and subsequent metallization etching displaying a high-density of small silver–silicon islands. A high rear illumination fill factor (FF) has been realized, although such high FF could also be a result of the lower short circuit current under rear illumination.

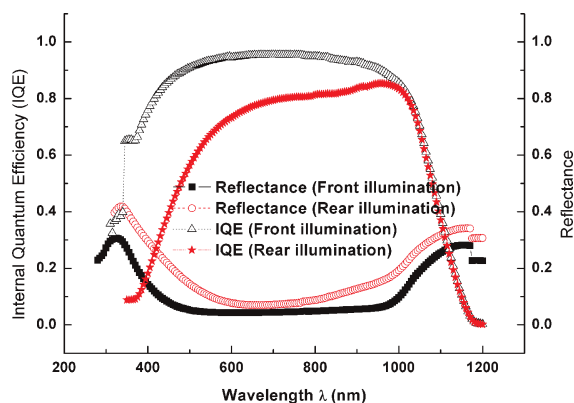
### 3. RESULTS AND DISCUSSION

Figure 2 shows the boron and phosphorus diffusion profiles at different drive-in temperatures. The carrier concentration after the boron diffusion (drive-in at 1020 °C) was  $\sim 6.5 \times 10^{19} \text{ cm}^{-3}$  and junction depth was  $\sim 0.7 \mu\text{m}$ . The junction depth for the phosphorus diffusion (driven-in at 950 °C) is  $\sim 0.4 \mu\text{m}$  with a surface carrier concentration of  $\sim 2.0 \times 10^{20} \text{ cm}^{-3}$ . We measured an implied  $V_{oc}$  value of 635 mV and effective lifetime ( $\tau_{eff}$ ) of 45  $\mu\text{s}$  after the diffusion steps.

The electrical parameters and  $I$ – $V$  curves for the bifacial solar cell are presented in Figure 4. Our fabricated bifacial



**Figure 4.** Front and rear electrical parameters and  $I$ – $V$  curve of the bifacial solar cell, measured at UCEP, Georgia Institute of Technology, under terrestrial standard testing conditions (STC).



**Figure 5.** Front and rear internal quantum efficiency (IQE) and reflectance of the bifacial solar cells.

solar cell on a  $2\ \Omega\text{cm}$  substrate produced front and rear energy conversion efficiencies of 16.6 and 12.8%, respectively. The ratio of the rear  $J_{\text{SC}}$  to front  $J_{\text{SC}}$  is 76.8%. The conversion efficiency of the bifacial cell under rear illumination is lower than the front because of lower short circuit currents ( $J_{\text{SC}}$ ) because of a higher rear surface reflectance (Figure 4). Recall that the silicon nitride thickness was not optimized for ARC but tailored to mask against phosphorus diffusion. Moreover, there is a 3% more metal coverage on the back side than the front, which adds to the total reflectance. Since upon rear illumination the junction is far from the sunward side, minority carriers generated near the rear of the device (blue and green spectral response) require long diffusion lengths in order to contribute to the short circuit current. In summary, the effective minority carrier lifetime, non-optimum silicon nitride layer, and 3% more metal coverage on the rear side are all responsible for the significantly lower rear illumination  $J_{\text{SC}}$ . The shunt resistance for both front and rear illuminations is high, indicative of the efficacy of the silicon nitride masking during phosphorus diffusion.

We have sacrificed the rear shading area by using the silver–aluminum paste for screen-printing the dilated fingers (final finger width is around  $130\ \mu\text{m}$  after firing process) at the  $\text{p}^+$  surface to balance the contact resistance and gridline resistance. The open circuit voltage (Figure 4) is consistent with  $45\text{-}\Omega/\text{sq}$  emitter in conjunction with Al–

**Table II.** Electrical parameters for the bifacial PV module in this study.

Electrical performance	Front surface	Rear surface
$P_{\text{max}}$ (W)	57.182	44.066
$V_{\text{oc}}$ (V)	17.863	16.837
$I_{\text{sc}}$ (A)	4.680	3.600
$V_{\text{pm}}$ (V)	13.931	13.927
$I_{\text{pm}}$ (V)	4.057	2.990



**Figure 6.** Appearance of the glass–glass, 30 bifacial cells PV module fabricated for this study.

BSF structure. To realize the potential of the bifacial cell with higher  $V_{\text{oc}}$ , more work is needed to understand how to tailor the boron diffusion profile and its associated  $\text{SiN}_x$  surface passivation to decrease the back saturation current ( $J_{\text{ob}}$ ).

Reflectance and internal quantum efficiency (IQE) curves under front and rear illuminations are presented in Figure 5. The difference between front and rear IQE in the short wavelength region is mainly due to the effect of bulk lifetime on minority carriers generated away from the collecting junction. As stated, rear reflectance is higher than that of the front side due to a 3% higher metal coverage as well as a non-optimized rear silicon nitride thickness on a planar rear surface.

Thirty bifacial solar cells were used to fabricate a glass–glass module. Table II shows the electrical parameters of the bifacial PV module, and the appearance of the module is shown in Figure 6. Outdoor performance of the bifacial PV module is now under monitoring and the cumulative performance will be reported in the future.

## 4. CONCLUSION

We have presented a screen-printed bifacial solar cell fabricated on p-type CZ monocrystalline silicon substrate. By optimizing the co-firing condition, high-density of silver crystallites at the  $\text{AgAl}/\text{Si}$  interface was obtained,

which produced low contact resistance. Fill factors of 0.772 for front illumination and 0.782 for illumination were measured. An open circuit voltage of 618 mV was obtained from front illumination, which matched the conventional Al-BSF solar cell with 45- $\Omega$ /sq emitter. An effective boron back surface field has been achieved using a silicon nitride effective in masking the phosphorus front emitter. The high shunt values achieved for both front and rear illuminations further supported the efficacy of the masking of the silicon nitride against phosphorus diffusion. We have thus obtained an efficiency of 16.6% from front illumination and 12.8% from the rear. To increase the efficiency ratio between the rear and front, more work is needed to understand the effect of boron diffusion depth, surface concentration, and passivation.

## ACKNOWLEDGEMENTS

This project is funded by the Natural Science Fund of Jiangsu Province, China.

## REFERENCES

- Narasimha S, Rohatgi A. Effective passivation of the low resistivity silicon surface by a rapid thermal oxide/plasma silicon nitride stack. *Applied Physics Letters* **72**: 1998; 1872–1874.
- Janßen L, Windgassen H, Bätzner DL, *et al.* Silicon solar cells passivated with silicon nitride. *23rd European Photovoltaic Solar Energy Conference*, Valencia, Spain, 1–5 September 2008; 1527–1529.
- Zhao J, Wang A, Altermatt P, Green MA. Twenty-four percent efficient silicon solar cells with double layer antireflection coatings and reduced resistance loss. *Applied Physics Letters* **66**: 1995; 3636–3638.
- Ebong AU, Lee SH, Honsberg CB, Wenham SR. Optimization of boron groove diffusion for double sided buried contact silicon solar cells. *25th IEEE Photovoltaic Specialists Conference*, 1996; 513–516.
- Recart F, Freire I, Pérez L, Lago-Aurrekoetxea R, Jimeno JC, Bueno G. Screen printed boron emitters for solar cells. *Solar Energy Materials and Solar Cells* **91**: 2007; 897–8902.
- Hilali MM, Gee JM, Hacke P. Bow in screen-printed back-contact industrial silicon solar cells. *Solar Energy Materials and Solar Cells* **91**: 2007; 1228–1233.
- Ghozati SB, Ebong AU, Honsberg CB, Wenham SR. Improved fill-factor for the double-sided buried—contact bifacial silicon solar cell. *Solar Energy Materials and Solar Cells* **51**: 1998; 121–128.
- Del Cañizo C, Moehlecke A, Zanesco I, Luque A. Cz bifacial silicon solar cells. *IEEE Electron Device Letters* **21**: 2000; 179–180.
- Janßen L, Windgassen H, Bätzner DL, *et al.* Silicon nitride passivated bifacial Cz–silicon solar cells. *Solar Energy Materials and Solar Cells* **93**: 2009; 1435–1439.
- Zhu JM, Shen WZ, Zhang YH, Dekkers HFW. Determination of effective diffusion length and saturation current density in silicon solar cells. *Solar Energy Materials and Solar Cells* **355**: 2005; 408–416.
- Orr Arienzo WA, Glang R, Lever RF, Lewis RK. Boron diffusion in silicon at high concentrations. *Journal of Applied Physics* **63**: 1988; 116.
- Ohe N, Tsutsui K, Warabisako T, Saitoh T. Effect of boron gettering on minority-carrier quality for FZ and CZ Si substrates. *Solar Energy Materials and Solar Cells* **48**: 1997; 145–150.
- Sinton RA, Cuevas A. Contactless determination of current–voltage characteristics and minority-carrier lifetimes in semiconductors from quasi-steady-state photoconductance data. *Applied Physics Letters* **69**: 1996; 2510–2512.
- Khadiolkar C, Sridharan S, Gnizak D, Pham T, Kim S, Shaikh A. Effect of glass chemistry and silicon orientation on the front contact microstructure formation in a silicon solar cell. *20th EU PSEC*, Barcelona, Spain, 2DV.2.1; 2005. pp. 1291–1296.
- Kerp H, Kim S, Lago R, *et al.* Development of screen-printable contacts for p<sup>+</sup> emitters in bifacial solar cells. *21st EU PSEC*, Dresden, 2CV.3.40; 2006.
- Ebong A, Kim DS, Yelundur V, *et al.* Understanding the role of forming gas on the screen-printed crystalline silicon solar cell front grid. *21st EU PSEC*, Dresden, 2DV.2.64; 2006.